EDGE ARTICLE

Check for updates

Crystals springing into action: metal–organic framework CUK-1 as a pressure-driven molecular spring†

Paul Iacomi, [a] Ji Sun Lee, [b] Louis Vanduyfhuys, [c] Kyung Ho Cho, [b]
Pierre Fertey, [d] Jelle Wieme, [c] Dominique Granier, [a] Guillaume Maurin, [a]
Veronique Van Speybroeck, [c] Jong-San Chang [b] and Pascal G. Yot *[a]

Mercury porosimetry and *in situ* high pressure single crystal X-ray diffraction revealed the wine-rack CUK-1 MOF as a unique crystalline material capable of a fully reversible mechanical pressure-triggered structural contraction. The near-absence of hysteresis upon cycling exhibited by this robust MOF, akin to an ideal molecular spring, is associated with a constant work energy storage capacity of 40 J g^{-1}. Molecular simulations were further deployed to uncover the free-energy landscape behind this unprecedented pressure-responsive phenomenon in the area of compliant hybrid porous materials. This discovery is of utmost importance from the perspective of instant energy storage and delivery.

Reducing the world's fossil fuel dependence is the focus of many global initiatives,[1] aiming to mitigate the effects of climate change through tapping into sustainable energy resources such as solar and wind power. However, increasing reliance on these renewable energy sources has introduced difficulties due to the offset between power availability and demand peaks. Complementary technologies are necessary to alleviate intermittent supply, such as peaking power plants, demand-side energy management, or large scale energy storage.[2] The latter is particularly desirable as it can decouple electricity production and consumption, however the lack of a "one size fits all" approach has led the scientific community to envisage unconventional energy storage strategies.

One such avenue emerging in recent years is the storage of mechanical energy *via* the compression of a suitable stimuli-responsive system, either through the intrusion of a non-wetting fluid into hydrophobic porous frameworks,[3] or by means of application of an external pressure on flexible materials.[4]

The former approach, first pioneered using water intrusion in zeolites and silicas,[11] has recently been extended to small pore zeolitic imidazolate frameworks.[12] Unfortunately, besides requiring highly hydrophobic systems, water intrusion achieves a relatively low stored energy density,[3] of around 3–25 J g^{-1}. The second strategy takes advantage of the compliant nature of bulk materials. Energy is stored through structural deformations, manifesting as continuous or sudden volume changes under external pressure. The energy stored in flexible materials over a compression/decompression cycle can be an order of magnitude higher compared to the values achieved using fluid intrusion in rigid porous systems.[13] In theory, three types of pressure-induced structural behaviour can be envisioned for such a responsive system. If the structure contraction is non-reversible, all energy is dissipated and the system is categorized as a nano-shock absorber (Fig. 1b). For structural changes that are reversible upon decompression two families of system can be distinguished, *i.e.* a nano-damper (Fig. 1c) or an ideal nano-spring (Fig. 1d) when the *p–V* curves show hysteresis or fully overlap, respectively.[14]

Metal–organic frameworks (MOFs), a class of porous, crystalline materials comprised of metal vertices interconnected by organic linkers, are known to exhibit responsiveness to a variety of stimuli,[15,16] including external pressure.[17] Recently, several frameworks of this family of hybrid materials have been shown to act as energy storing nano-dampers or energy dissipative nano-shock absorbers, as is the case for the highly flexible MIL-53(M)[5,8,10] and MIL-47(V)[9] series and more recently ZIF-4(Zn)[7] (see Fig. 1b and c for their related structural behaviours). In such flexible crystalline materials compression is associated with a displacive phase transition between distinct structures of differing unit cell volumes, denoted as open (op) and contracted (cp) forms[15,16] and illustrated in Fig. 1a, occurring reversibly or

[a] ICGM, University Montpellier, CNRS, ENSCM, F-34095 Montpellier, France. E-mail: pascal.yot@umontpellier.fr; Fax: +33 4 67 14 42 90; Tel: +33 4 67 14 32 94

[b] Research Center for Nanocatalysts, Korea Research Institute of Chemical Technology, Yusung, Daejeon 305-600, Korea

[c] Centre for Molecular Modeling, Ghent University, Technologiepark 903, B-9052 Zwijnaarde, Belgium

[d] Synchrotron Soleil, L'orme des Merisiers, Saint-Aubin - BP 48, F-91192 Gif-sur-Yvette cedex, France
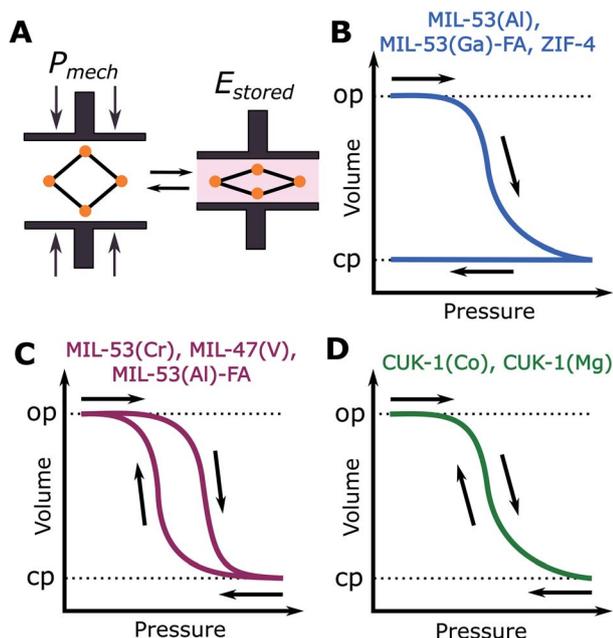
Fig. 1 (A) Schema of mechanical energy storage in compliant crystalline materials, implying a unit cell volume change between open (op) and contracted (cp) structures, and prototypical pressure-volume curves of stimuli-responsive materials under mechanical pressure for (B) nano-shock absorbers, exemplified by MIL-53(Al),[5] MIL-53(Ga)-FA[6] and ZIF-4(Zn),[7] (C) nano-dampers *e.g.* MIL-53(Cr),[8] MIL-47(V)[9] and MIL-53(Al)-FA[10] and (D) nano-springs, insofar exhibited exclusively by CUK-1 presented herein.

irreversibly for a nano-damper or nano-shock absorber, respectively. The considerable stored energy associated with this transition, in the range of 30–200 J g^{-1} (up to 4 kJ g^{-1} for shock absorbers[18]) is highly attractive from the perspective of mechanical energy storage. However, the hysteretic compression/decompression curve characterising known nano-damper MOFs leads to a partial loss of work energy, lowering the potential storage efficiency, as well as creating issues through heat dissipation. Insofar, the search for a ideal spring-like crystalline material, capable of reversible pressure-induced structural switching without any hysteresis (Fig. 1d) has been fruitless, precluding their applicability for efficient, high density energy storage applications. Herein, a subtle combination of Hg-porosimetry, high-pressure single crystal X-ray diffraction (SC-XRD) and molecular simulations reveals the 1D-channel CUK-1 (M, M = Co, Mg)[19] MOF as the first compliant hybrid porous material with a spring-back mechanical breathing behaviour.

Such unique mechanically-triggered structural response implies a continuous pore contraction/expansion between op and cp forms in a narrow pressure range of 280–290 MPa, accompanied by a unit cell volume change of 20.9%. This optimal scenario paves the way towards fast energy storage/delivery system of about 40 J g^{-1}. The channel-like CUK-1(M) composed of chains of μ_3-OH/O edge and vertex sharing metal octahedra (M = Co,[19] Mg[20]) coordinated by bidentate 2,4-pyridinedicarboxylic ligands, recently emerged as an attractive

porous material owing to its promising sorption performance combined with environmentally-friendly hydrothermal synthesis and high thermal and chemical stability.[20–22] Its wine-rack topology and its relatively rigid behaviour upon guest adsorption are reminiscent to that of MIL-47(V) a MOF which interestingly underwent a hysteretic, reversible structural contraction upon exerting an external pressure of 125 MPa,[9] associated with a stored/delivered energy of 33 J g^{-1}. Inspired by our previous findings on MIL-47(V), we deliberately explored the pressure-induced structural behaviour of CUK-1 in its iso-structural Co and Mg forms. MOF synthesis was performed according to the protocol detailed in ESI.† Phase purity was confirmed by powder XRD (Fig. S3, S4 and Table S1†) while their textural features, including BET area and pore volume, were found to match previously reported data.[19,20]

Mercury intrusion curves were recorded on the powder samples up to a maximum of 413 MPa as shown for CUK-1(Co) in Fig. 2, its Mg variant being reported in Fig. S6, ESI,† together with full experimental details. A substantial amount of Hg intrudes at low pressure (<10 MPa), due to compaction of the crystals and filling of inter-particle porosity. This is followed by a sudden volume change at 281 MPa where a sharp step is observed (see inset of Fig. 2). By analogy with the conclusions previously drawn for the series of MIL-53(M)/MIL-47(V) frameworks,[5,8–10] this intruded Hg volume increase is associated with a structural contraction of CUK-1(Co), as its channel size (approx. 6.6 Å) is an order of magnitude below the pore dimension where non-wetting mercury can intrude in this pressure range (at 52 Å). The extrusion curve shows a near-perfect overlap, indicating that the framework behaves as an ideal spring, with no hysteresis between the intrusion/extrusion branches.

Moreover, this behaviour is highly repeatable, as confirmed by four consecutive pressure cycles (in Fig. S5†). Interestingly, the same behaviour also holds true for CUK-1(Mg) (Fig. S6†),
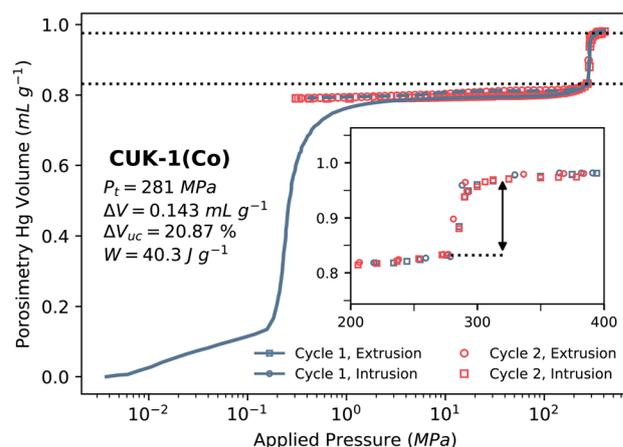

Fig. 2 Sequential mercury intrusion–extrusion curves on CUK-1(Co) powder, in blue line and red, respectively. Line is a guide for eye. Volume below 1 MPa corresponds to powder compaction and inter-crystallite void filling. Dotted horizontal lines demarcate contraction lower and upper bounds. Inset highlights the intrusion step in a linear scale with the op/cp contraction marked with an arrow.

with a similar intrusion pressure of 288 MPa. Since the two metal ions show relatively similar ionic radius (Co^{2+}: 1.50(7) Å and Mg^{2+}: 1.41(7) Å),[24] the averaged metal–oxygen distance is nearly identical in their corresponding coordination: spheres: (Co–O: 2.107(20) Å and Mg–O: 2.073(20) Å). Such analogous metal-linker bond strength is most likely at the origin of the very similar pressure-induced response of the two materials. The high transition pressure of CUK-1(Co) underpins the inability of guest adsorption to induce a breathing effect as observed previously.[20,21] Indeed, the adsorption stresses encountered throughout guest insertion are simply insufficient to overcome the energetic penalty of transition.[14,25] The 0.143 mL g^{-1} volume change associated with the observed step in the CUK-1(Co) intrusion curve corresponds to a 20.9% change in unit cell volume, lower than in the similar phenyl-based MIL-47(V) of 43%.[9] However, the stored energy calculated through $W = P \times \Delta V$ is 40 J g^{-1}, 20% larger than the value reported for MIL-47(V)[9] of 33 J g^{-1}. Here, the higher pressure of CUK-1(Co) switching, 281 MPa vs. 125 MPa for MIL-47(V) balances out the ΔV term. Moreover, owing to its relatively dense framework, the volumetric energy density of CUK-1(Co) remains attractive when compared to water intrusion systems (Table S4†).

Considering an initial unit cell volume for the CUK-1(Co) op form of 2467 Å^3 from PXRD (see ESI†), the resulting cp form is estimated to exhibit a unit cell volume of 1950 Å^3, based on the Hg intruded volume increase at 281 MPa. In order to directly observe the contracted form and identify the mechanism underpinning these intriguing dynamics, high pressure SC-XRD experiments were carried out in a membrane diamond anvil cell (mDAC). Individual CUK-1(Co) crystals were placed in a gasket between the polished diamonds of the mDAC, and immersed in a hydrostatic pressure transmitting medium of silicone oil AP-100, with a gold flake used to monitor inner mDAC pressure (full single crystal synthesis conditions and SC-XRD methodology available in the ESI†).

At ambient pressure, the indexed unit cell volume of the initial op form of CUK-1(Co) is nearly identical (2492 Å^3) to that of the previously reported[20] dehydrated monoclinic phase (2466.72 Å^3). Upon increasing DAC pressure to around 0.3 GPa, a volume contraction to the cp phase begins, which is in line with Hg porosimetry experiments. Reflections obtained from integrated 2D diffraction images were used to solve the pressure-induced structure through a dual space recycling algorithm in an expanded P1 setting, then further refined on F^2 using the SHELX suite[26] (complete data treatment methodology available in the ESI†). The structure maintains the same $C2/c$ space group throughout the transition between the two forms, and as such the spring-like dynamics of the framework can be described as a continuous contraction in a narrow pressure range. Above 0.5 GPa, the cp form is attained, with further pressure application leading to a linear decrease of its unit cell volume by 4% up to 1.8 GPa (Fig. 3).

The unit cell dimensions of the solved cp form at 0.5 GPa are provided in Table 1, alongside as-indexed pristine op form parameters with Fig. 4a illustrating the two structures. The anisotropic transition is similar in nature to that of MIL-53(M)/ MIL-47(V), characterised by a compaction in the b-direction (from approx. 13 Å to 9 Å) and an elongation along the a-axis (from 18 to nearly 20 Å). The change in the c-parameter is minimal, with only a slight increase, as it lies in the plane of the highly rigid octahedrally coordinated metal chains. A lowering of the angle (from 103 to 99°) is also observed, as the 1D parallel pores are straightened via the linker-induced torsion. A table comparing specific atomic distances, angles and torsions in the two forms is available in Table S7, ESI.† The unit cell volume of the identified cp phase at 0.5 GPa of 1972 Å^3 is only slightly higher than the value estimated from porosimetry measurements (as 1950 Å^3). We attribute this offset to the different interactions of the crystal surface with the respective pressure transmitting medium (mercury vs. silicone oil), as observed previously.[5]

A careful inspection of the op/cp structures suggests that the unique spring-like behaviour of the CUK-1 framework under pressure can be related to the position and concerted motion of its linkers upon compaction. The asymmetric linker coordination of the pyridine nitrogen to the Co–O chains results in a dual-hinged pivot, while the opposing carboxylic group adopts a single hinge configuration as in MIL-53 (H' and H in Fig. 4b).

In conjunction with alternating connectivity in both the b and c-crystallographic axes, as depicted in Fig. 4c, the
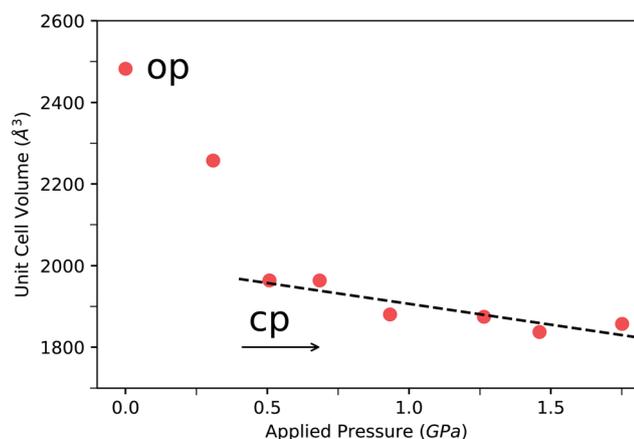

Fig. 3 Evolution of the CUK-1(Co) unit cell volume determined through indexation of Bragg reflections as a function of applied pressure as recorded in a DAC. Unit cell parameters corresponding to each pressure point can be found in Table S5, ESI.†

Table 1 Crystallographic data of the pristine (op) and high pressure (cp) phases as determined from the CUK-1(Co) SC-XRD

Form	op^a	cp^b
Crystal system	Monoclinic	Monoclinic
Space group	$C2/c$ (no. 15)	$C2/c$ (no. 15)
a (Å)	18.024(15)	19.6026(9)
b (Å)	13.089(3)	9.2017(9)
c (Å)	10.883(13)	11.0368(3)
β (°)	103.92(12)	99.434(3)
Unit cell volume (Å^3)	2492(4)	1963.8(2)

^{a} As indexed before pressure application. ^{b} As solved at 0.5 GPa, R_{int} = 3.08, R_1 = 5.53, wR_2 = 16.51.
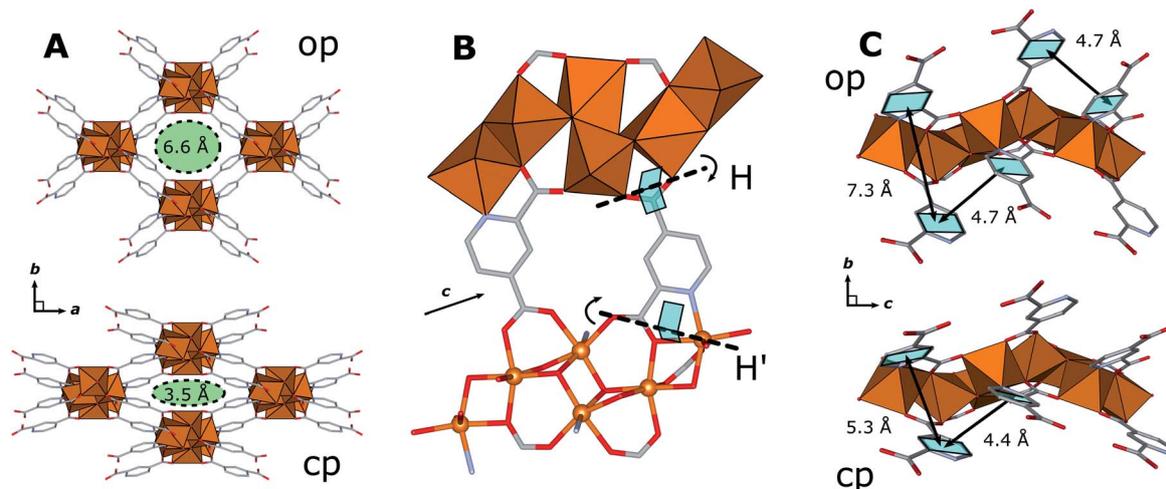
Fig. 4 (A) Comparison of the structures of the op and cp forms of CUK-1(Co), corresponding to applied pressure of 0 GPa and 0.5 GPa, respectively, with corresponding pore limiting diameters. (B) Close-up of two adjacent linkers coordinated to the metal chains, highlighting their pivoting motion: [H] a carboxylic group hinge, with the O−O axis acting as a kneecap identical to that of MIL-53(Cr),[23] and [H'] a dual carboxylic group − pyridine nitrogen hinge with the axis of rotation offset through the Co atom. (C) Concerted linker motion displayed alongside the c axis, highlighting the phenyl–phenyl distances in the two forms. Cobalt atoms/tetrahedra, oxygen, carbon and nitrogen atoms are depicted in orange, red, light grey and light blue, respectively, with hydrogen atoms omitted for clarity.

corrugated channels maintain a similar separating distance between adjacent linkers throughout contraction (4.7 Å to 4.4 Å). The aromatic stacking interactions are therefore much weaker than those encountered between facing phenyl rings in the cp forms of MIL-53(M)/MIL-47(V), (separating distances lower than 4 Å) which all show irreversible or hysteretic behaviours upon pressure release.[8–10] Such a conformation is expected to lower the relative stability of the cp form of CUK-1, rendering possible a complete reversibility of the cp/op transition.

In order to gain further insight into the mechanical behaviour of CUK-1, we computed the internal energy of CUK-1(Mg) as a function of unit cell volume at 0 K using density functional theory (DFT) calculations. The Mg variant was chosen for this computational investigation because Co is a transition

metal with a high spin state in CUK-1 resulting in an electronic structure that is much more difficult to resolve using standard DFT. The calculations were performed using the Vienna *Ab initio* Simulation Package (VASP)[27] with the PBE-D3(BJ)[28,29] functional (details in the ESI†) and the results are shown in Fig. 5.

The profile reveals a single minimum located at around 2500 $Å^3$ which can hence be identified as the op form. No local minimum is present at a lower unit cell volume, which is consistent with the experimental observation of a pressure-induced reversible contraction. However, the profile does exhibit an inflection point in the volume range of 1800–2000 $Å^3$, which fits with the dimension of the cp form observed experimentally. As was mentioned before, dispersion interactions between stacking aromatic linkers has been put forward as the driving force for structural transitions in MOFs such as MIL-53(Al). In previous theoretical work[30] it was concluded that the contribution of dispersion to the DFT energy difference between the op and cp states of MIL-53(Al) heavily depends on the applied level of theory, making it very difficult to make quantitative statements about dispersion contribution from DFT calculations at this point. However, we herein assume we can still make a qualitative comparison between two different materials (*i.e.* MIL-53(Al) and the present CUK-1) using the same level of theory. In this light, we found from the aforementioned theoretical work that the dispersion contribution for MIL-53(Al) at the PBE-D3(BJ) level of theory amounts to 138 J g^{-1} (145 kJ mol^{-1} per unit cell) which is responsible for stabilizing the cp state ultimately resulting in an irreversible transition. In the present case of CUK-1, our DFT calculations using the same functional showed that the contribution of the dispersion to the energy difference between the op state (chosen at 2500 $Å^3$) and the cp state (chosen at 1900 $Å^3$) is only 84 J g^{-1} (110 kJ mol^{-1} per
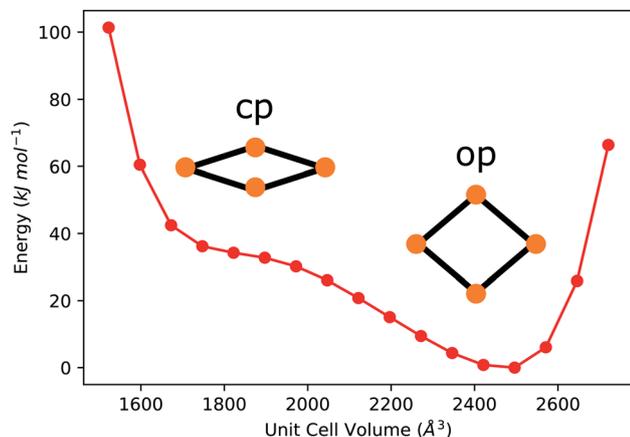

Fig. 5 Internal energy of the CUK-1(Mg) framework as a function of its unit cell volume at 0 K computed at the DFT level.

unit cell). As the dispersion contribution for CUK-1 is much lower than for MIL-53(Al), we can interpret this as a lower degree of stabilization of the cp form. This, in combination with the deformation energy required for the linker staggering that was mentioned before and illustrated in Fig. 4, prevents the contracted form from being a metastable state and hence promotes the ideal spring-like behaviour.

As the energy profile exhibits an inflection point at the contracted pore volume range, a volume *versus* pressure response derived from this profile would reveal hysteresis in the transition pressures, which is not in agreement with the ideal-spring behaviour observed experimentally. However, the DFT profile was computed at 0 K, while the experiments were performed at room temperature. Therefore, we derived a force field for CUK-1(Mg) using QuickFF[31] (more details on the force field derivation can be found in the ESI†) and computed the free energy at 300 K as a function of unit cell volume from molecular dynamics simulations using a protocol outlined in earlier work.[14] The corresponding pressure profile (shown in Fig. S8a of the ESI†) indicates a reversible transition lacking any hysteresis, in excellent agreement with the experimentally observed ideal-spring behaviour for this solid. Finally, upon decomposing the free energy into internal energy and entropy (see Fig. S8b of the ESI†), we found that the entropic contributions stabilize the op phase (or equivalently destabilize the cp phase), which further enhances the ideal spring-like behaviour.

Conclusions

We have shown that CUK-1 in its Co and Mg forms undergoes a fully reversible pressure induced contraction, analogous to a nano-spring, the first known compliant hybrid porous material to display this spectacular behaviour. The large system volume change of 20%, observed in a narrow range of pressure (280–290 MPa) by Hg hydrostatic compression experiments has been fully elucidated *in situ* as a displacive phase transformation to a contracted phase, a transition capable of storing 40 J g^{-1} of work energy. Our synchronous computational investigation demonstrates that while dispersion linker stacking interactions still play a role in the system's switchability, entropic stabilisation and a staggered linker configuration mediate the free energy landscape to yield a spring-like response. This discovery opens a new direction in the design of soft metamaterials, capable of instant energy storage. Further understanding of the fundamental role of various building blocks and topologies in the emergence of pressure responsive nanosprings is expected to allow precise fine-tuning of potential storage capacity.

Author contributions

JSL, KHC and JSC synthesized the samples. PI and PGY prepared cells at Soleil Synchrotron. PGY and PI carried out mercury intrusion. DG performed PXRD laboratory powder X-ray diffraction and PGY performed Rietveld refinements at selected temperatures. PI, PF and PGY performed single crystal X-ray diffraction at Synchrotron Soleil and refined the crystal structures. LV, JW, GM and VVS performed the molecular simulations. PI, LV, GM, VVS, JSC, and PGY contributed to the manuscript preparation.

Conflicts of interest

The authors declare no conflict of interest.

Acknowledgements

Notes and references

1 M. Z. Jacobson and M. A. Delucchi, *Sci. Am.*, 2009, **301**, 58–65.

2 O. Palizban and K. Kauhaniemi, *J. Energy Storage*, 2016, **6**, 248–259.

3 G. Fraux, F.-X. Coudert, A. Boutin and A. H. Fuchs, *Chem. Soc. Rev.*, 2017, **46**, 7421–7437.

4 F. A. Hill, T. F. Havel, D. Lashmore, M. Schauer and C. Livermore, *Energy*, 2014, **76**, 318–325.

5 P. G. Yot, Z. Boudene, J. Macia, D. Granier, L. Vanduyfhuys, T. Verstraelen, V. Van Speybroeck, T. Devic, C. Serre, G. Férey, N. Stock and G. Maurin, *Chem. Commun.*, 2014, **50**, 9462–9464.

6 P. Ramaswamy, J. Wieme, E. Alvarez, L. Vanduyfhuys, J.-P. Itié, P. Fabry, V. Van Speybroeck, C. Serre, P. G. Yot and G. Maurin, *J. Mater. Chem. A*, 2017, **5**, 11047–11054.

7 S. Henke, M. T. Wharmby, G. Kieslich, I. Hante, A. Schneemann, Y. Wu, D. Daisenberger and A. K. Cheetham, *Chem. Sci.*, 2018, **9**, 1654–1660.

8 I. Beurroies, M. Boulhout, P. L. Llewellyn, B. Kuchta, G. Férey, C. Serre and R. Denoyel, *Angew. Chem., Int. Ed.*, 2010, **49**, 7526–7529.

9 P. G. Yot, Q. Ma, J. Haines, Q. Yang, A. Ghoufi, T. Devic, C. Serre, V. Dmitriev, G. Férey, C. Zhong and G. Maurin, *Chem. Sci.*, 2012, **3**, 1100.

10 P. G. Yot, L. Vanduyfhuys, E. Alvarez, J. Rodriguez, J.-P. Itié, P. Fabry, N. Guillou, T. Devic, I. Beurroies, P. L. Llewellyn, V. Van Speybroeck, C. Serre and G. Maurin, *Chem. Sci.*, 2016, **7**, 446–450.

11 V. Eroshenko, R.-C. Regis, M. Soulard and J. Patarin, *J. Am. Chem. Soc.*, 2001, **123**, 8129–8130.

12 A. U. Ortiz, A. Boutin, A. H. Fuchs and F.-X. Coudert, *J. Chem. Phys.*, 2013, **138**, 174703.

13 F. A. Hill, T. F. Havel and C. Livermore, *Nanotechnology*, 2009, **20**, 255704.

14 L. Vanduyfhuys, S. M. J. Rogge, J. Wieme, S. Vandenbrande, G. Maurin, M. Waroquier and V. Van Speybroeck, *Nat. Commun.*, 2018, **9**, 204.

15 S. Kitagawa, R. Kitaura and S. Noro, *Angew. Chem.*, 2004, **43**, 2334–2375.

16 G. Férey, *Chem. Soc. Rev.*, 2008, **37**, 191–214.

17 L. R. Redfern, L. Robison, M. C. Wasson, S. Goswami, J. Lyu, T. Islamoglu, K. W. Chapman and O. K. Farha, *J. Am. Chem. Soc.*, 2019, **141**, 4365–4371.

18 Y.-R. Miao, Z. Su and K. S. Suslick, *J. Am. Chem. Soc.*, 2017, **139**, 4667–4670.

19 S. M. Humphrey, J.-S. Chang, S. H. Jhung, J. W. Yoon and P. T. Wood, *Angew. Chem., Int. Ed.*, 2007, **46**, 272–275.

20 B. Saccoccia, A. M. Bohnsack, N. W. Waggoner, K. H. Cho, J. S. Lee, D.-Y. Hong, V. M. Lynch, J.-S. Chang and S. M. Humphrey, *Angew. Chem., Int. Ed.*, 2015, **54**, 5394–5398.

21 E. Sánchez-González, P. G. M. Mileo, M. Sagastuy-Breña, J. R. Álvarez, J. E. Reynolds, A. Villarreal, A. Gutiérrez-Alejandre, J. Ramírez, J. Balmaseda, E. González-Zamora, G. Maurin, S. M. Humphrey and I. A. Ibarra, *J. Mater. Chem. A*, 2018, **6**, 16900–16909.

22 S.-J. Lee, J. L. Mancuso, K. N. Le, C. D. Malliakas, Y.-S. Bae, C. H. Hendon, T. Islamoglu and O. K. Farha, *ACS Mater. Lett.*, 2020, 499–504.

23 C. Serre, F. Millange, C. Thouvenot, M. Nogues, G. Marsolier, D. Louër and G. Férey, *J. Am. Chem. Soc.*, 2002, **124**, 13519–13526.

24 B. Cordero, V. Gómez, A. E. Platero-Prats, M. Revés, J. Echeverría, E. Cremades, F. Barragán and S. Alvarez, *Dalton Trans.*, 2008, 2832.

25 F.-X. Coudert, *Bull. Jpn. Soc. Coord. Chem.*, 2019, **73**, 15–23.

26 G. M. Sheldrick, *Acta Crystallogr., Sect. A: Found. Adv.*, 2015, **71**, 3–8.

27 G. Kresse and J. Furthmüller, *Phys. Rev. B: Condens. Matter Mater. Phys.*, 1996, **54**, 11169–11186.

28 J. P. Perdew, K. Burke and M. Ernzerhof, *Phys. Rev. Lett.*, 1996, **77**, 3865–3868.

29 S. Grimme, J. Antony, S. Ehrlich and H. Krieg, *J. Chem. Phys.*, 2010, **132**, 154104.

30 J. Wieme, K. Lejaeghere, G. Kresse and V. Van Speybroeck, *Nat. Commun.*, 2018, **9**, 4899.

31 L. Vanduyfhuys, S. Vandenbrande, T. Verstraelen, R. Schmid, M. Waroquier and V. Van Speybroeck, *J. Comput. Chem.*, 2015, **36**, 1015–1027.